ADVANCED FUNCTIONAL MATERIALS
www.afm-journal.de

Remotely Controlled Red Blood Cell Carriers for Cancer Targeting and Near-Infrared Light-Triggered Drug Release in Combined Photothermal–Chemotherapy

*Xiaoqi Sun, Chao Wang, Min Gao, Aiyan Hu, and Zhuang Liu**

Red blood cells (RBCs), the "innate carriers" in blood vessels, are gifted with many unique advantages in drug transportation over synthetic drug delivery systems (DDSs). Herein, a tumor angiogenesis targeting, light stimulus-responsive, RBC-based DDS is developed by incorporating various functional components within the RBC platform. An albumin bound near-infrared (NIR) dye, together with a chemotherapy drug doxorubicin, is encapsulated inside RBCs, the surfaces of which are modified with a targeting peptide to allow cancer targeting. Under stimulation by an external NIR laser, the membrane of the RBCs would be destroyed by the light-induced photothermal heating, resulting in effective drug release. As a proof of principle, RBC-based cancer cell targeted drug delivery and light-controlled drug release is demonstrated in vitro, achieving a marked synergistic therapeutic effect through the combined photothermal–chemotherapy. This work presents a novel design of smart RBC carriers, which are inherently biocompatible, promising for targeted combination therapy of cancer.

1. Introduction

Addressing the pharmacokinetic limitations, improving therapeutic efficiency and reducing side effects of drugs during clinical pharmacotherapy is a long-standing challenge in drug development.[1–3] With the improvement of drug delivery systems (DDSs), significant progresses have been made in recent years. Generally, the following important aspects should be considered in the development of DDSs.[4] First, the carriers should have good biocompatibility. Second, they could circulate for a long time in the bloodstream with favorable pharmacokinetic index after systemic administration. Third, they should be able to specifically target the lesion to improve drug efficacy and reduce side effects. Fourth, the controllable release at the desired time and location should be realized. DDSs currently available or under investigations are mostly synthetic carriers,[2,5,6] many of which, however, may not be able to fully satisfy clinical expectations because of their lack of biocompatibility or unsatisfied pharmacokinetic parameters. Recently, cell-based drug delivery systems, along with various kinds of bio-inspired, bioengineered, and biomimetic drug delivery carriers, have received great attention for a dream that DDSs could be designed to be as smart as live cells while behaving in a controllable manner.[4,7,8]

Red blood cells (RBCs), the "innate carriers" in our blood vessels for oxygen transportation, have a long history of being investigated for drug delivery.[9–11] As "innate carriers," they are endowed with many unique characteristics: (1) perfect biocompatibility, (2) long circulating half-life (≈120 days in humans), (3) membrane flexibility and stability, (4) the absence of nucleus, organelles, and DNA (without tumorigenicity), (5) high surface to volume ratio (beneficial for surface modification). Many pioneering explorations in this field have been reported starting from 1970s.[7,12–15] In the past two years, the development of RBC-based DDSs has regained increasingly high interests,[16–22] particularly in combination with newly developed nanotechnology and nanomedicine.[17,19,22,23] For examples, Anselmo et al. reported that noncovalently attaching nanoparticles to the surface of RBCs could allow transient accumulation of nanoparticles in the lung, while reducing their uptake by liver and spleen.[17] In our recent work, RBCs are attached with magnetic nanoparticles and loaded with two types of therapeutic agents for magnetic field enhanced in vivo combination therapy of cancer.[19] However, there are still a number of limitations when RBC-based delivery of chemotherapeutics are used in cancer treatment: (1) Considering the micrometer sizes of RBCs, those carriers could hardly penetrate blood vessels and reach tumor cells, even if tumor vasculatures are rather leaky. (2) Since intact RBC membrane is impermeable to many drug molecules, the drug release from RBCs is usually via slow diffusion through the RBC plasma membrane and/or the graduate degradation of RBCs.[4,12] Therefore, an alternative approach may be designing a smart RBC carrier which binds to tumor blood vessels, and then releases drug molecules specifically inside the tumor upon certain stimulations.

In recent years, smart DDSs which are responsive to external stimuli such as light, magnetic field, electric field, and ultrasound, have received significant attention, as these systems

X. Sun, Dr. C. Wang, M. Gao, A. Hu, Prof. Z. Liu
Institute of Functional Nano and Soft Materials (FUNSOM), Collaborative Innovation Center of Suzhou Nano Science and Technology
The Jiangsu Key Laboratory for Carbon-Based Functional Materials and Devices
Soochow University
Suzhou 215123, P.R. China
E-mail: zliu@suda.edu.cn

DOI: 10.1002/adfm.201500061

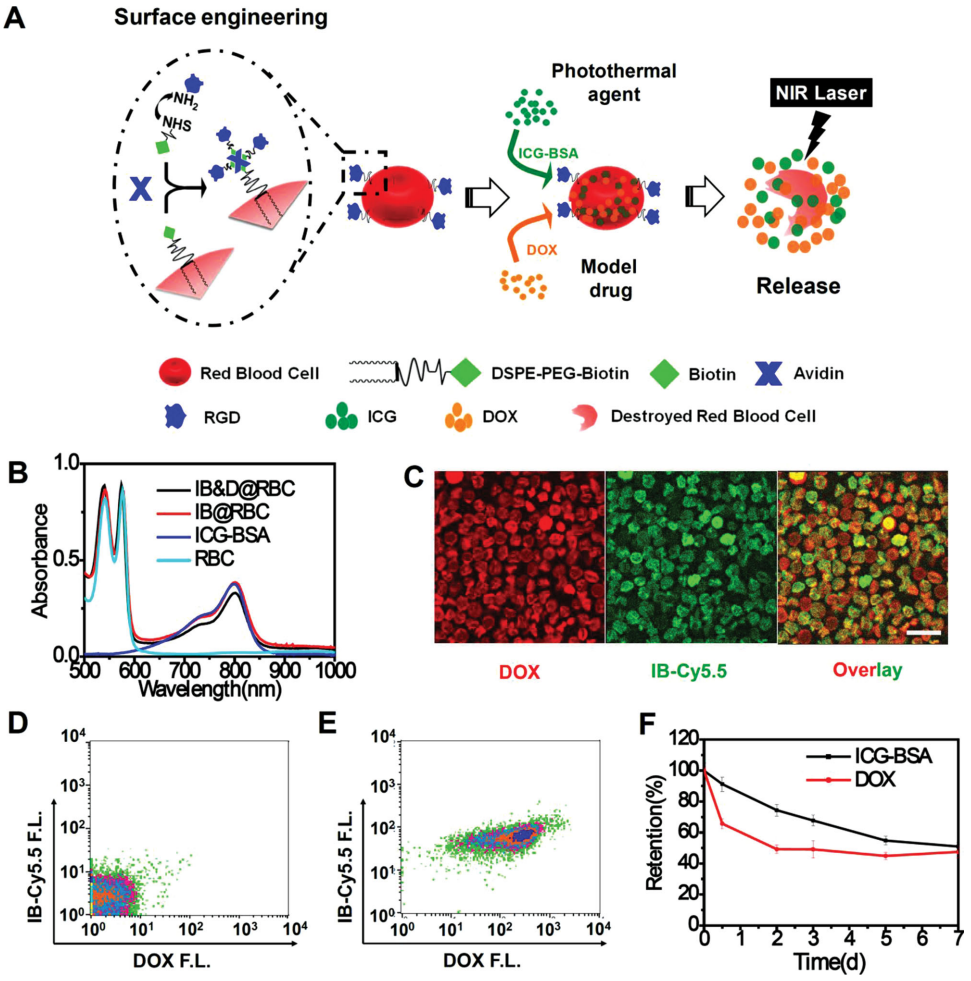

Figure 1. Preparation and characterization of multifunctional RBC carriers. A) Schematic illustration to show the fabrication of tumor angiogenesis-targeting RBC–RGD, the subsequent loading with drug and photothermal agents, and the remotely controlled drug release under NIR laser. B) UV–vis–NIR absorbance spectra of RBC, ICG–BSA, IB@RBC, and IB&D@RBC. The peak at ≈800 nm evidenced the successful loading of ICG–BSA into RBCs. C) Confocal images of IB-Cy5.5&D@RBC–RGD. Fluorescence of DOX and IB-Cy5.5 showed obvious colocalization inside RBCs. The scale bar is 5 μm. Flow cytometry data of D) native RBC and E) IB-Cy5.5&D@RBC–RGD. Flow cytometry data proved that most RBCs were successfully loaded with DOX and IB-Cy5.5. F) Release of DOX and ICG–BSA from IB&D@RBCs over time. Both DOX and ICG–BSA showed slow and steady release from RBCs. Error bars were based on standard deviation (SD) of triplicate samples. Note that Cy5.5 was introduced for BSA labeling only to facilitate confocal imaging (C) and flow cytometry measurement (D,E), but not used in other parts of this work.

can increase drug release at targeted lesions through a more specific manner, decrease systemic toxicity, and potentially avoid under- or overdosing.[24–26] Among various stimuli, near-infrared (NIR) light (700–900 nm) is regarded as an attractive one because of its noninvasiveness, the ability to penetrate reasonably deep tissues, and easy of manipulation to irradiate a focused, selected lesion region.[27–29] Inspired by NIR-induced photothermal destruction of tumor cells,[30–34] we thus wonder whether drug-loaded RBC carriers can be disrupted by heating under laser irradiation to realize controlled release in the tumor site if photothermal agents are coencapsulated into RBCs together with chemotherapeutics. Therefore, in this article, we design a NIR light stimulus–response RBC carrier with tumor angiogenesis targeting ability. As shown in **Figure 1**A, our RBCs are first modified with RGD (Arg–Gly–Asp) peptide, which targets the hallmark of tumor angiogenic endothelium $\alpha_v\beta_3$-integrin. Then a model drug, doxorubicin (DOX), and a photothermal agent, indocyanine green–bovine serum albumin nanocomplex (ICG–BSA), are coencapsulated into engineered RBCs (IB&D@RBC–RGD). Under NIR irradiation, those RBCs could be heated up, resulting in a controlled burst drug release (≈80% of release within 5 min). As a proof-of-principle, RBC-based targeted drug delivery and remotely controlled drug release is demonstrated in vitro using a $\alpha_v\beta_3$-integrin positive U87MG cell line, achieving a marked synergistic therapeutic efficacy through combined photothermal–chemotherapy.

2. Results and Discussion

Hypotonic dialysis, a most commonly used method to load drug molecules or other theranostic agents inside RBCs,[35] was employed in our experiments. In brief, a suspension of fresh RBCs was mixed with molecular payloads and dialyzed against

a hypotonic buffer at 4 °C. After that, the swollen RBCs containing desired payloads were transferred to a hypertonic buffer and dialyzed at 37 °C to reconstitute osmotic pressure and reseal those molecules inside RBCs. Adenosine triphosphate (ATP), glutathione (GSH), and some metabolic intermediates were added to help maintaining the structure of RBCs and protecting them from oxidative damage.

As shown in Figure 1A, to realize NIR laser-induced release, a NIR photothermal agent should be encapsulated inside RBCs. ICG, a FDA-approved small molecular dye with strong NIR absorbance,[36–38] was initially chosen in our experiment. However, during the experiment of encapsulating ICG into RBCs, we found that ICG molecules could be adsorbed on the membrane of RBCs and then were easily washed away by serum-supplemented medium. Such rapid release of ICG from RBCs was not ideal for further applications. It has been found that albumin proteins could form nanocomplexes with many organic dye molecules[39,40] including ICG (Figure S1, Supporting Information). We thus wondered whether the complex of ICG with BSA could be loaded into RBCs with better stability. Therefore, ICG–BSA (IB) was loaded into RBCs by the hypotonic dialysis method. The UV–vis–NIR absorption spectrum was examined for the obtained ICG–BSA loaded RBCs (IB@RBCs), which showed a strong ICG absorption peak at ≈800 nm (Figure 1B). Compared to RBCs loaded with free ICG, ICG in the IB@RBC sample was much more stable and showed a rather slow release (Figure S1E, Supporting Information).

Based on that, a model drug, DOX, was coencapsulated into RBCs together with ICG–BSA via the same hypotonic dialysis method. The characteristic ICG absorbance peak was again observed for RBCs loaded with dual types of agents (IB&D@RBCs) (Figure 1B). As no suitable laser was available to excite ICG–BSA in our confocal fluorescence microscope and flow cytometry instrument, BSA was covalently labeled with a red fluorescent dye Cy5.5 to allow tracking of BSA inside RBCs. As shown in Figure 1C, obvious colocalization of Cy5.5 and DOX fluorescence was observed in confocal images of RBCs loaded with both Cy5.5-labeled IB and DOX, suggesting successful coencapsulation of these two agents inside RBCs. Flow cytometry data (Figure 1D,E) further confirmed that most of RBCs after such hypotonic dialysis treatment were coloaded with both DOX and ICG-BSA. As quantified by UV–vis–NIR absorbance (ICG–BSA absorption peak) and fluorescence emission spectra (DOX fluorescence), it was estimate that ≈1.8×10^7 ICG and ≈6.6×10^7 DOX molecules were loaded inside each RBC (Figure S2, Supporting Information). Given all the results described above, the ICG–BSA and DOX coencapsulated RBCs were successfully fabricated.

We then carefully examined the properties of our engineered RBCs. Suspensions of native RBCs, DOX-loaded RBCs (D@RBC), IB@RBC, and IB&D@RBC all showed favorable dispersity while the color of IB@RBC and IB&D@RBC turned into slightly darker owing to the existence of encapsulated ICG–BSA in those samples (Figure S3, Supporting Information). It is well-established that phosphatidylserine (PS) exposure is involved in recognition and removal of damaged and senescent RBCs by the reticuloendothelial system (RES).[41,42] Therefore, we evaluated PS exposure of our RBC carriers by Annexin V binding assay (Figure S4, Supporting Information). To eliminate interference of DOX fluorescence to FITC–Annexin V analysis, here we used the RBC carrier experienced the same encapsulating procedure without drugs to evaluate the damage to RBCs caused by our loading conditions. In the flow cytometry data, PS exposure ratio of RBC carriers was 1.8%, much lower than that of RBC ghost (78%), indicating that the encapsulation procedures in our experiments did not cause significant damages to the membrane structure of RBCs. As for the release behaviors, we found that both DOX and ICG–BSA exhibited slow release kinetics within seven days (Figure 1G). Since ICG complexed with BSA had a larger size compared to small DOX molecules, the release of ICG from RBCs appeared to be much slower than that of DOX. Notably, the morphology of our engineered IB&D@RBC carriers remained largely intact even after being stored for seven days (Figure S3, Supporting Information).

ICG with strong NIR absorbance has been demonstrated to be an effective photothermal agent. We next wondered whether NIR laser-induced photothermal effect would be able to trigger drug release from our engineered RBC carriers. Both native RBCs and IB&D@RBC at the same cell concentration were exposed to an 808-nm NIR laser under different power densities. An infrared (IR) thermal camera was used to record the temperature change during laser irradiation. (**Figure 2**A) As shown in Figure 2B, with the increase of laser power density from 0.1 to 0.5 W cm^{-2}, the final temperature of IB&D@RBC suspensions after 5 min laser irradiation increased from ≈34 to ≈50 °C. In contrast, the final temperature of native RBC suspension was only ≈32 °C even after laser irradiation at 0.5 W cm^{-2} for 5 min.

Confocal microscope images were then taken for those engineered RBCs after photothermal heating (Figure 2C). Without laser irradiation (0 W cm^{-2}), the fluorescence of DOX was confined inside RBCs. As the increase of laser power density (from 0.1 to 0.5 W cm^{-2}), RBCs gradually lost their regular morphologies after NIR-induced photothermal heating, which in the meanwhile triggered obvious drug release from RBCs as revealed by the appearance of strong DOX fluorescence outside cells. Note that significant self-quenching of DOX fluorescence was observed when those molecules were encapsulated inside RBCs (Figure S5, Supporting Information). After laser irradiation under 0.5 W cm^{-2} for 5 min, RBCs were completed destructed while DOX release was the most obvious. The exact ratio of light-triggered drug release was then determined by measuring DOX fluorescence in the supernatant of irradiated samples. Consistent to confocal data, increased DOX release was observed from IB&D@RBC as the rise of laser power densities (Figure 2D). As much as ≈80% of DOX was released after the IB&D@RBC sample was exposed to the 808-nm laser at 0.5 W cm^{-2} for 10 min (Figure 2D,E). In marked contrast, less than 10% of DOX release was observed for D@RBC under the same laser irradiation condition (Figure 2E), owing to the absence of significant photothermal effect in this sample without ICG. Therefore, NIR laser could be utilized as an external stimulus to effectively and precisely control the drug release from our RBC-based DDS at the desired time and localization.

Considering their micrometer sizes which limit the extravascular diffusion of RBCs, engineering tumor vasculature targeted RBCs may be a realistic approach to develop cancer-targeted

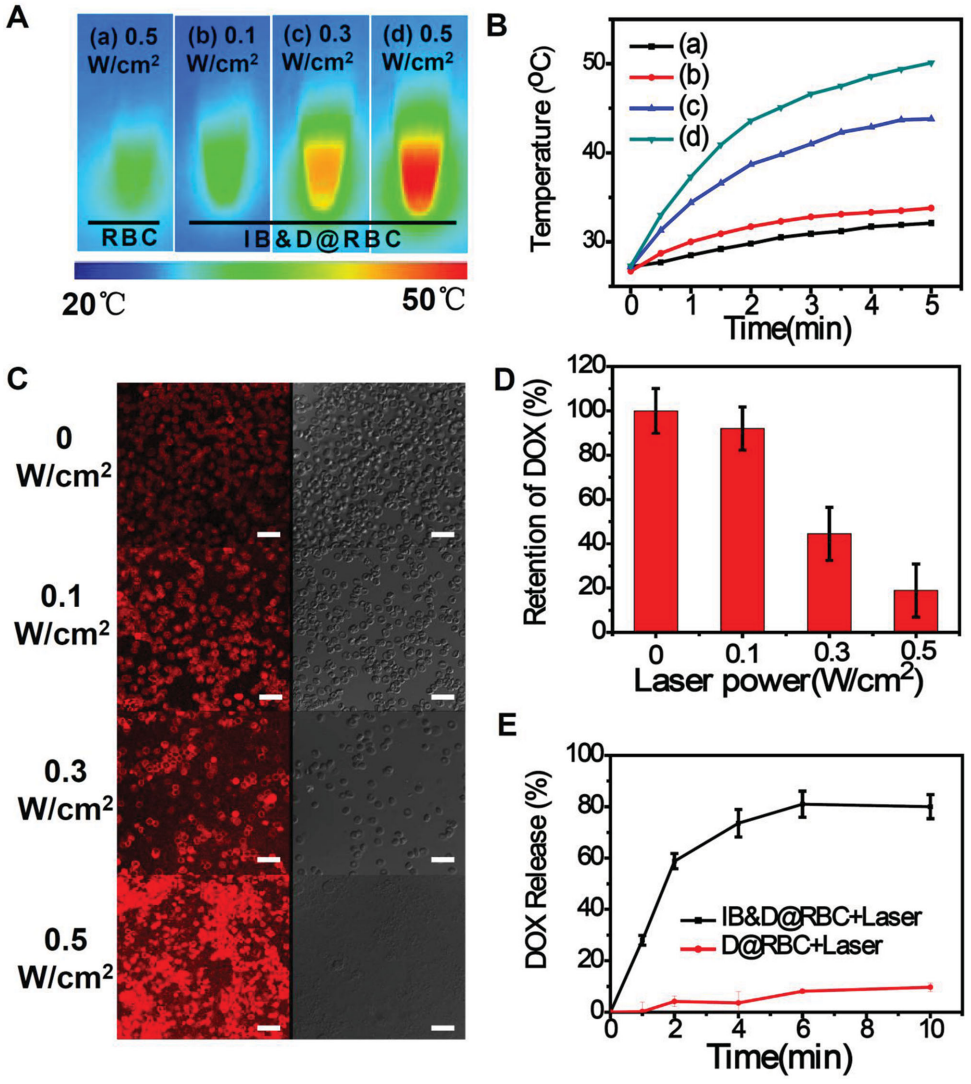

Figure 2. Photothermal properties and NIR light-triggered drug release of IB&D@RBC. A) IR thermal images and B) heating curves of IB&D@RBC suspension under NIR laser irradiation with different power densities. C) Confocal images of IB&D@RBC after laser irradiation at different power densities for 10 min. The scale bars are 20 μm. D) Quantitative detection of NIR-triggered release of DOX from IB&D@RBC carriers (samples in (C)). Error bars are based on triplicate measurements. With the increase of laser power density, more RBCs were destroyed, resulting in enhanced DOX release. E) Kinetics of NIR-triggered release. The samples were irradiated with NIR laser at the power density of 0.5 W cm^{-2}. Error bars are based on triplicate measurements.

DDSs based on RBCs. Therefore, RGD (Arg–Gly–Asp) peptide, which could bind with $\alpha_v\beta_3$-integrin overexpressed on angiogenic tumor vasculature endothelium cells, was gifted on the RBC surface to impart them cancer targeting ability. Here, we used a gentle and efficient surface engineering strategy to attach ligands to the surface of RBCs. In our experiments, RBCs were mixed with biotin conjugated poly(ethylene glycol)–distearoyl phosphatidylethanolamine (DSPE–PEG–biotin), whose lipid chains could be inserted into the lipid bilayer of RBC membrane to allow stable anchoring of biotin on RBCs. It was estimated that each RBC was conjugated with ≈6.30×10^4 biotin molecules after such treatment (Figure S6, Supporting Information). Those biotinylated RBCs were modified with avidin, a specific biotin-binding protein with four binding sites on each protein. The leftover binding sites on avidin were then conjugated with biotinylated RGD, forming RGD-modified RBCs (RBC–RGD).

In this system, the flexible PEG spacer could allow more efficient interaction of RGD and the $\alpha_v\beta_3$-integrin receptors on tumor cells, while the multivalent avidin–(biotin–RGD)$_3$ structure may be favorable to achieve high binding affinity. Such method without touching proteins on RBC plasma membrane appeared to be a gentle method that induced no appreciable damage to RBCs. After the surface engineering, we incubated the engineered RBCs in the autologous serum. As shown in Figure S7, Supporting Information, the engineered RBCs show no obvious hemolysis in fresh autologous serum, indicating no harmful effect during our RGD conjugation steps to complement-controlling proteins on the membrane (decay accelerating factor, DAF, and CD59).[43] Besides, we also evaluated

PS exposure of our engineered RBCs by Annexin-V binding assay, and found that the PS exposure ratio of our RBC–RGD was rather low (Figure S4, Supporting Information). Preliminary in vivo results indicated that those RGD-modified RBCs after intravenous injection into mice showed rather long blood circulation time, further confirming that surface modification of RBCs by our method would not significantly alter the physiological stability of RBCs (Figure S8, Supporting Information).

Afterward, the specific $\alpha_v\beta_3$-integrin binding ability of our RGD-modified RBCs was tested in vitro by incubating RBC–RGD with two types of cancer cells, U87MG ($\alpha_v\beta_3$-integrin positive) and 4T1 ($\alpha_v\beta_3$-integrin negative) cells. Native RBCs without RGD modification were used as the control. Unbound RBCs were removed by washing after 30 min of incubation. Remarkably, U87MG cells with upregulated $\alpha_v\beta_3$-integrin expression were fully covered by numerous RGD-modified RBCs, while very few native RBCs were attached to U87MG cells. In contrast, 4T1 cells which were negative in $\alpha_v\beta_3$-integrin expression could not be recognized by RBC–RGD (**Figure 3**). Blocking experiment by pretreating U87MG cells with excess free RGD could inhibit the binding of RBC–RGD on U87MG cells, further confirming the specific tumor cell recognition ability of our engineered RBCs (Figure 3c). Therefore, RBCs after RGD modification via our method, on one hand showed intact membrane structure, on the other hand could specifically target $\alpha_v\beta_3$-integrin overexpressed on tumor vasculatures as well as several types of cancer cells.

To mimic the desired in vivo procedure in which circulating RBC carriers selectively accumulate in the tumor site and release their payload under NIR irradiation, we designed a proof-of-principle in vitro experiment to demonstrate this concept. In our experiment, two types of cancer cells (U87MG and 4T1) were incubated with IB&D@RBC–RGD or IB&D@RBC without RGD modification for 30 min. After removal of unattached RBCs, those cancer cells were exposed to the 808-nm laser at 0.5 W cm^{-2} for 10 min (**Figure 4**A). Several other controls including U87MG cells incubated with IB&D@RBC–RGD but without laser exposure, U87MG cells incubated with free DOX at the equivalent concentration, as well as RGD-blocked U87MG cells incubated with IB&D@RBC–RGD and with laser treatment, were also included in our experiments. Confocal fluorescence imaging and flow cytometry analysis were carried out 2 h later after removing RBCs by a red blood cell lysis solution. As expected, strong DOX fluorescence was observed inside U87MG cells treated with IB&D@RBC–RGD and after laser exposure, while cells in the other groups showed much weaker DOX uptake as revealed by both confocal imaging results and flow cytometry data. Our results demonstrated that the molecular targeting in combination with NIR-triggered drug release could greatly facilitate drug uptake by cancer cells.

Finally, a targeted photothermal–chemotherapy was demonstrated. U87MG cells were incubated with IB&D@RBC without RGD modification, IB@RBC–RGD without DOX loading, as well as IB&D@RBC–RGD, for 30 min. After removal of unattached RBCs, the cells were exposed to NIR laser irradiation (808 nm, 0.3 W cm^{-2}, 20 min) and then further incubated for another 24 h. Calcein–AM/propidium iodide (PI) costaining (**Figure 5**A) and standard cell viability assay (Figure 5B) were carried out afterward to evaluate the cancer cell killing efficacy. Compared to cells treated with IB&D@RBC + laser, a significantly improved therapeutic effect was observed for cells treated with IB&D@RBC–RGD + laser, owing to the specific binding of RGD-modified RBCs on U87MG cells. On the other side, comparing the groups of IB@RBC–RGD + laser, IB&D@RBC–RGD without laser, and IB&D@RBC–RGD + laser, an obvious synergetic cancer cell killing effect was achieved with the combined photothermal and chemotherapy in the last group, in which the majority of cancer cells were destructed after incubation with IB&D@RBC–RGD and exposure to NIR laser. Such synergetic cancer killing resulted from not only the laser-induced hyperthermia effect, but also the NIR laser-triggered DOX release. Note that free DOX as the same concentration and experimental condition was not as effective to kill those cells (Figure 5B). All those results collectively suggest that our engineered RBCs (IB&D@RBC–RGD) after specific binding to $\alpha_v\beta_3$-integrin positive cancer cells could release DOX upon NIR laser irradiation and then induce effective cancer cell killing.

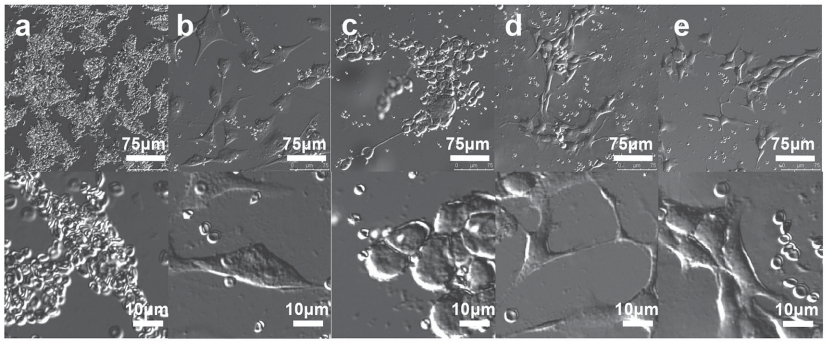

Figure 3. Specific cancer cell targeting of the engineered RBC carriers. Confocal images of U87MG cells incubated with a) RBC–RGD, b) native RBCs, c) RGD blocked U87MG cells incubated with RBC–RGD, and 4T1 cells incubated with d) RBC–RGD, and e) native RBCs. All the groups experienced 30 min of incubation and washing to remove unbound RBCs. As shown in the images, $\alpha_v\beta_3$-integrin positive U87MG cells were fully covered by RGD conjugated RBCs but not native RBCs or RGD-blocked U87MG cells. Such effect was also not noted for $\alpha_v\beta_3$-integrin negative 4T1 cells. In the blocking group, the morphology of U87MG cells changed after blocking of $\alpha v\beta 3$-integrin by RGD (20 μg mL^{-1} for 30 min).

3. Conclusion

In summary, we have successfully fabricated a smart RBC carrier suitable for targeted drug delivery and light-controlled release for cancer therapy. In our system, various functioning components were incorporated within RBCs, including the function of NIR laser triggering release from ICG–BSA, the targeting function from RGD, and the therapy function from the model drug

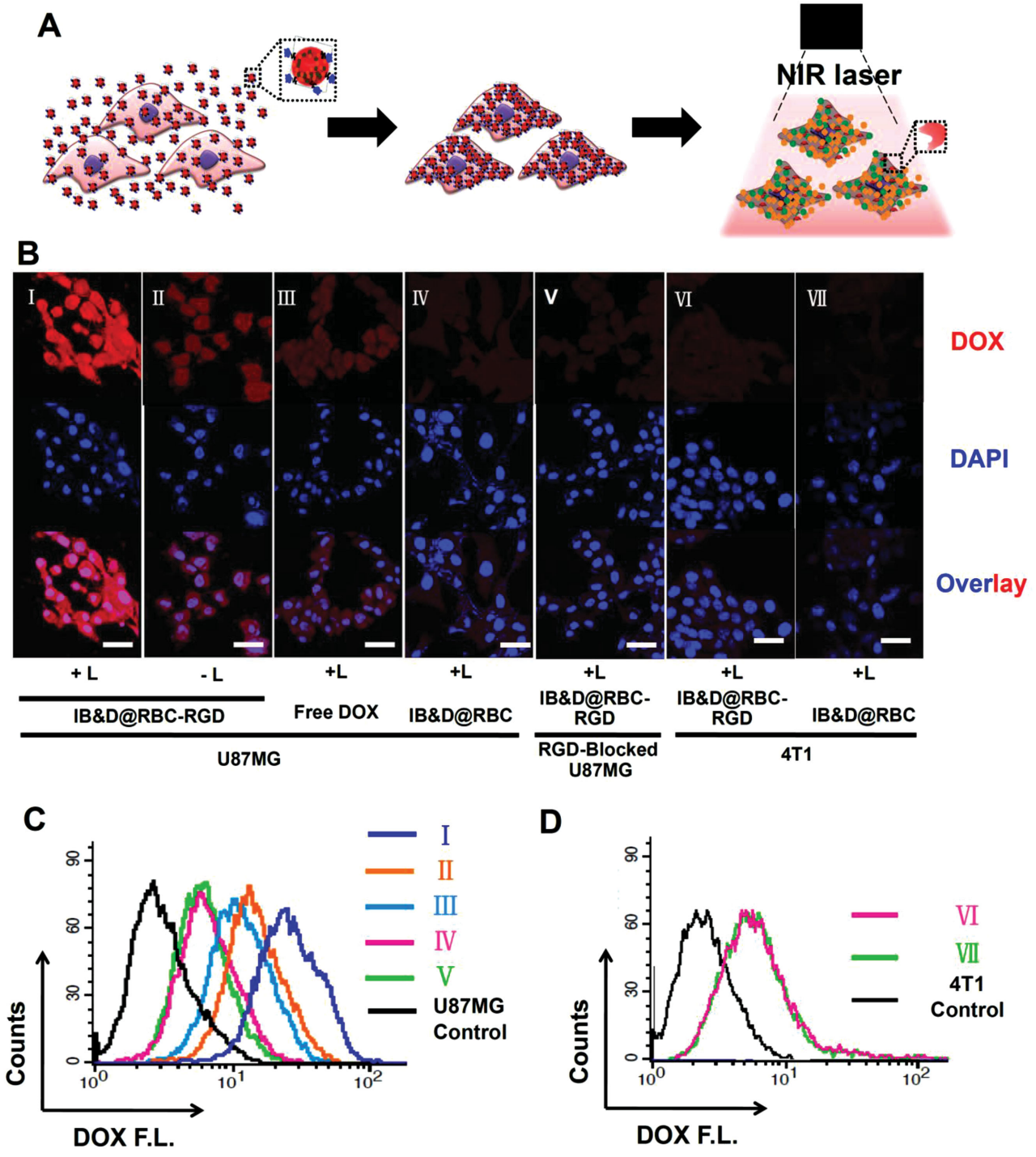

Figure 4. In vitro targeted drug delivery and light-triggered release. A) Schematic illustration of in vitro targeted drug delivery and photothermally triggered drug release. B) Confocal fluorescence images of U87MG cells incubated with IB&D@RBC–RGD, IB&D@RBC, or free DOX for 30 min, followed by removing unattached RBC, being exposed to NIR laser irradiation (808 nm, 0.5 W cm^{-2}, 10 min) or without laser irradiation, and then further incubation for 2 h. RGD-blocked U87MG cells were involved as the control. Red and blue colors in those images represent DOX fluorescence and 40-6-diamidino-2-phenylindole (DAPI)-stained nuclear fluorescence, respectively. The scale bars are 35 μm in all confocal images. C,D) Flow cytometry data of cellular DOX fluorescence for samples in (B). Cells were treated with red blood cell lysis solution to remove RBCs attached on the U87MG cell surface before imaging and analysis.

DOX. With intact RBC membrane and being stable in dark, those engineered RBCs when under NIR laser irradiation could be disrupted and then release their encapsulated drug molecules. After modifying RBCs with RGD peptide, specific binding of RBCs to $\alpha_v\beta_3$-integrin overexpressing cancer cells is then observed. Afterward, in vitro targeted drug delivery

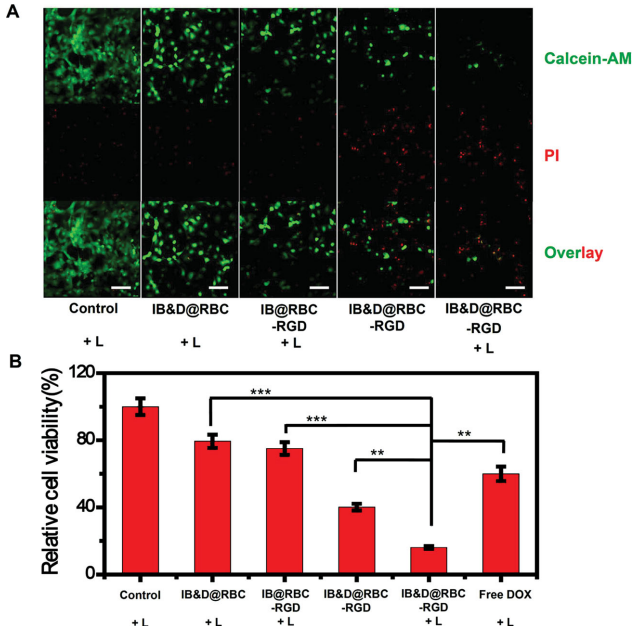

Figure 5. In vitro combined photothermal–chemotherapy. A) Confocal images of U87MG cells treated with laser only, IB&D@RBC + laser, IB@RBC–RGD+ laser, IB&D@RBC–RGD, and IB&D@RBC–RGD+ laser. Laser treatment was conducted by an 808 nm laser at 0.3 W cm^{-2} for 20 min. U87MG cells were incubated with RBCs for 30 min followed by removing unattached RBC, being exposed to NIR laser irradiation (808 nm, 0.3 W cm^{-2}, 20 min) and then incubating for another 20 h. The scale bars are 100 μm in all confocal images. B) Relative viabilities of U87MG cells in (A). The data are shown as mean ± SD. Error bars are based on at least quadruplicate measurements. *p* values: ***$p < 0.001$, **$p < 0.01$, or *$p < 0.05$.

and photothermal–chemotherapy are further conducted, demonstrating a remarkable synergistic therapeutic effect after the targeted combination therapy delivered by RBCs. For further in vivo studies and future potential clinical translation, $\alpha_v\beta_3$-integrin targeting RBCs may specifically bind to tumor vasculature endothelia, and then release chemotherapeutic agent under external NIR laser irradiation to destruct cancer vasculature as well as tumor cells. Animal studies in mouse tumor models are still ongoing in our laboratory. Noteworthily, all the agents used here to engineer our RBC platform are either FDA-approved or highly biocompatible. Although the limited light penetration depth would be a shortcoming of this approach, it is hoped that such light-responsive DDSs may become clinical applicable with the aid of intervention techniques (e.g., use implantable optical fibers). Moreover, the similar strategy may be further extended to the development of other types of stimulus–response RBC-based DDSs suitable for the treatment of extravascular diseases in addition to cancer.

4. Experimental Section

Preparation of IB&D@RBC: IB&D@RBC was prepared based on an optimized "hypotonic dialysis" method.[35,44] Essential steps of the process involved collection and washing of erythrocytes, dialysis of erythrocytes against a hypotonic buffer, resealing drug insides erythrocytes, and removing unencapsulated drug. Briefly, whole blood was collected from the orbital sinus of Babl/c mice. RBCs were separated from whole blood by centrifugation (400 g, 10 min), washed thrice with cold PBS (300 mOsm, pH 7.4), and then resuspended in PBS buffer at a 70% hematocrit. 200 μL suspension of RBCs was then placed inside a dialysis bag with a 3.5 kDa molecular weight cut-off (MWCO) together with 1 mL mixture of DOX and ICG–BSA containing 1 mg mL^{-1} DOX and 60 mg mL^{-1} ICG–BSA (with 1 mg mL^{-1} of ICG). The dialysis medium was 100 mL hypotonic buffer (pH 7.4) containing 10×10^{-3} M $NaHCO_3$, 10×10^{-3} M NaH_2PO_4, 20×10^{-3} M glucose, 4×10^{-3} M $MgCl_2$, 2×10^{-3} M ATP, and 3×10^{-3} M reduced glutathione (GSH). Hypotonic dialysis was carried out at a temperature of 4 °C for 30 min. Resealing of RBCs was obtained by dialyzing RBCs in a hypertonic solution containing 10% PIGPA–NaCl (a specialized buffer, including 100×10^{-3} M Natrium pyruvat, 100×10^{-3} M Inosin, 100×10^{-3} M Glucose, 35×10^{-3} M NaH_2PO_4, 5×10^{-3} M Adenin, and 12% (w/v) NaCl), 2×10^{-3} M ATP, and 3×10^{-3} M GSH at 37 °C for 30 min. The resealed cells were recovered by centrifugation at 400 g and washed four times with ice-cold PBS to remove unentrapped drugs.

Surface Modification of RBC: RBC surface modification is realized by the surface painting method.[20] DSPE–PEG–biotin was synthesized by mixing 35 mg DSPE–PEG–NH_2 (3400 D) and 7 mg NHS–biotin (341 D, 2 eq) within 5 mL methanol and reacting for 2 h, followed by blowing dry by N_2, dialyzing against DI water using 3500 D MWCO membranes, and freeze-drying. To prepare biotin anchored RBCs, 500 μL packed RBCs were resuspended in 4 mL PBS (pH 7.4) and incubated with 0.5 mg DSPE–PEG–biotin (3700 D,100 μg mL^{-1}) for 30 min at 37 °C under continuous stirring. The obtained RBC–biotin were washed twice (PBS, pH 7.4, 400 g, 5 min) and then resuspended in 4 mL PBS (pH 7.4). Under continuous stirring, 1 mg avidin solution (6.30×10^4 molecules/RBC) was added and reacted for 60 min at 4 °C. Afterward, the RBC–biotin–avidin were washed twice (PBS, pH 7.4, 400 g, 5 min) to remove unbound avidin. Finally, washed RBC–biotin–avidin was mixed with biotinylated RGD (resulted from the reaction of RGD and sulfo–NHS–LC–biotin) for 60 min at 4 °C under continuous stirring, washed twice with PBS, and then stored under 4 °C for further use. The number of biotin anchored on each RBC was quantified by fitting an avidin binding curve on biotinylated RBCs. In briefly, avidin was labeled with NHS–FITC in advance. Under continuous vibration, samples of biotinylated RBCs with a fixed cell number were added with varied amounts of avidin–FITC and incubated for 60 min under 4 °C. After removal of unattached avidin–FITC, the relative levels of avidin binding on RBCs in those samples were determined by flow cytometry. Based on the fluorescence of RBCs and avidin/RBC number ratios, an avidin binding plot was drawn. After fitting the curve, we could get the saturated avidin binding number for each RBC at the turning point. The number of biotin copies attached per RBC could thus be inferred from this saturated avidin binding number.

Characterization of Loaded RBCs: Confocal fluorescence images of cells were taken by a Lecia SP5 laser scanning confocal microscope. For flow cytometry measurement, RBCs were washed with PBS twice and then analyzed using a Calibur flow cytometer (BD Biosciences, USA). To determine the DOX loading, which could not be accurately estimated by the UV–vis spectrum due to the interference of hemoglobin absorption, a quantitative DOX cell uptake assay was thus conducted by solubilizing engineered RBCs using a lysis buffer and then extracting free DOX from the cell lyate by an HCl/isopropanol solvent. The fluorescence of DOX was then used to determine DOX loading inside RBCs. Plain RBCs without DOX loading or IB-loaded RBCs were treated by the same method and used as the baseline control during DOX measurement (Figure S2, Supporting Information). The amount of ICG–BSA loading on RBCs was measured by the characteristic ICG–BSA absorbance at 802 nm in the engineered RBC sample, after subtracting the inherent RBC absorbance at that wavelength. Carrier-RBC membrane damage (PS exposure) was quantified using FITC–Annexin V assay according to the manufacturer's instructions (FITC–Annexin V Apoptosis Detection Kit, Sigma-Aldrich). The results were analyzed by flow cytometry (BD Biosciences, USA). To evaluate hemolysis by complement, engineered

RBCs were incubated in fresh serum for 1 h at 37 °C. The degree of hemolysis was judged by observation and spectrophotometrical determination of released hemoglobin at 405 nm. To determine drug releasing from engineered RBCs, DOX and ICG–BSA released from IB&D@RBC–RGD were collected by centrifugation at 1000 rpm for 10 min. The amounts of released DOX and ICG–BSA in the supernatant solutions were measured by fluorescence and absorbance spectra, respectively. The DOX samples were extracted by an HCl/isopropanol solvent, while the ICG–BSA samples were solubilized by a lysis buffer.

Photothermal Release Experiments: To study the photothermal property of IB&D@RBC, suspensions of 10% hematocrit RBCs and IB&D@RBC were irradiated under an 808-nm laser at 0.1, 0.3, and 0.5 W cm^{-2} for 5 min with an IR thermal camera used to monitor their temperature changes during laser irradiation. NIR laser-induced photothermal release was conducted at different power densities of NIR laser irradiation. Confocal fluorescence images of irradiated cells were taken by a Lecia SP5 laser scanning confocal microscope. The excitation wavelength was 488 nm for DOX.

Cell Culture Experiments: Human glioblastoma U87MG cells were cultured in DMEM low glucose medium containing 10% fetal bovine serum (FBS) and 1% penicillin/streptomycin at 37 °C under 5% CO_2. Murine breast 4T1 cancer cells were cultured in RPMI-1640 medium containing 10% FBS and 1% penicillin/streptomycin at 37 °C under 5% CO_2. For targeted therapy, 50 µL of 30% hematocrit IB&D@RBC-RGD ($\approx 1 \times 10^8$) added with 1% penicillin/streptomycin was mixed with U87MG cells or 4T1 cells cultured in 35 mm dishes. After 30 min of incubation, RBCs were removed by washing twice with fresh culture medium. Afterward, those samples were placed under the 808 nm laser irradiation at 0.5 W cm^{-2} for 10 min. After additional incubation for 2 h, the samples were stained with 4′,6-diamidino-2-phenylindole (DAPI) and examined by the Lecia SP5 confocal fluorescence microscope or the Calibur flow cytometer. RBCs attached on cancer cells were fully lyzed by treating with RBC lysis solution (NH_4Cl) twice (2 min each time) before examination. The control groups were treated with parallel operations.

In Vitro Photothermal–Chemotherapy: Five groups were designed in our experiments: (1) U87MG + laser, (2) U87MG + IB&D@RBC+ laser, (3) U87MG + IB@RBC–RGD+ laser, (4) U87MG + IB&D@RBC–RGD, (5) U87MG + IB&D@RBC–RGD+ laser. For groups (2)–(5), 50 µL of 30% hematocrit RBCs containing 1% penicillin/streptomycin was added into each 35 mm culture dish with U87MG cells. After 30 min of incubation, the free engineered RBCs were removed by washing twice with fresh culture medium. Afterward, those samples were exposed to the 808-nm laser at 0.3 W cm^{-2} for 20 min and then further incubated for additional 24 h. In the control groups, parallel operations were conducted. For confocal fluorescence investigation, dead and live cells were stained with propidium iodide (PI, 5×10^{-3} M) and calcein AM (2×10^{-3} M), respectively. The in vitro therapeutic effect was also determined using a standard methyl thiazolyl tetrazolium (MTT, Sigma Aldrich) assay for cell viability measurement. Briefly, U87MG cells were seeded into 96-well cell culture plate at 1×10^4 per well until adherent and then incubated with 5 µL 30% hematocrit of RBCs (1×10^7) or 0.6 µg free DOX. All the other operations were the same as described before. Error bars were based on standard deviations of at least quadruplicate measurements.

Supporting Information

Supporting Information is available from the Wiley Online Library or from the author.

Acknowledgements

This work was partially supported by the National Basic Research Programs of China (973 Program) (2012CB932600, 2011CB911002), the National Natural Science Foundation of China (51222203, 51132006), a Jiangsu Natural Science Fund for Distinguished Young Scholars (BK20130005), and a Project Funded by the Priority Academic Program Development (PAPD) of Jiangsu Higher Education Institutions. For the animal experiments, Balb/c mice were purchased from Nanjing Peng Sheng Biological Technology Co Ltd (China) and used under protocols approved by Soochow University Laboratory Animal Center.

Received: January 6, 2015
Published online: February 25, 2015

[1] T. M. Allen, P. R. Cullis, *Science* **2004**, *303*, 1818.
[2] J.-W. Yoo, D. J. Irvine, D. E. Discher, S. Mitragotri, *Nat. Rev. Drug Discov.* **2011**, *10*, 521.
[3] T. A. Kolesnikova, A. G. Skirtach, H. Möhwald, *Exp. Opin. Drug Deliv.* **2013**, *10*, 47.
[4] F. Pierige, S. Serafini, L. Rossi, M. Magnani, *Adv. Drug Deliv. Rev.* **2008**, *60*, 286.
[5] R. van der Meel, L. J. Vehmeijer, R. J. Kok, G. Storm, E. V. van Gaal, *Adv. Drug Deliv. Rev.* **2013**, *65*, 1284.
[6] T. M. Allen, P. R. Cullis, *Adv. Drug Deliv. Rev.* **2013**, *65*, 36.
[7] M. A. Fischbach, J. A. Bluestone, W. A. Lim, *Sci. Transl. Med.* **2013**, *5*, 179.
[8] X. Zhang, X. Zeng, X. Liang, Y. Yang, X. Li, H. Chen, L. Huang, L. Mei, S.-S. Feng, *Biomaterials* **2014**, *35*, 9144.
[9] E. Beutler, G. Dale, D. Guinto, W. Kuhl, *Proc. Natl. Acad. Sci. USA* **1977**, *74*, 4620.
[10] K. Kinosita, T. Y. Tsong, *Nature* **1978**, *272*, 258.
[11] G. M. Ihler, R. H. Glew, F. W. Schnure, *Proc. Natl. Acad. Sci. USA* **1973**, *70*, 2663.
[12] V. R. Muzykantov, *Exp. Opin. Drug Deliv.* **2010**, *7*, 403.
[13] C. G. Millan, M. L. Marinero, A. Z. Castaneda, J. M. Lanao, *J. Controlled Release* **2004**, *95*, 27.
[14] M. Hamidi, A. Zarrin, M. Foroozesh, S. Mohammadi-Samani, *J. Controlled Release* **2007**, *118*, 145.
[15] M. Hamidi, A. Zarrin, M. Foroozesh, S. Mohammadi-Samani, *J. Controlled Release* **2007**, *118*, 145.
[16] C. F. Greineder, M. D. Howard, R. Carnemolla, D. B. Cines, V. R. Muzykantov, *Blood* **2013**, *122*, 1565.
[17] A. C. Anselmo, V. Gupta, B. J. Zern, D. Pan, M. Zakrewsky, V. Muzykantov, S. Mitragotri, *ACS Nano* **2013**, *7*, 11129.
[18] G. Ferrauto, D. Delli Castelli, E. Di Gregorio, S. Langereis, D. Burdinski, H. Grüll, E. Terreno, S. Aime, *J. Am. Chem. Soc.* **2013**, *136*, 638.
[19] C. Wang, X. Sun, L. Cheng, S. Yin, G. Yang, Y. Li, Z. Liu, *Adv. Mater.* **2014**, *26*, 4794.
[20] R. Mukthavaram, G. Shi, S. Kesari, D. Simberg, *J. Controlled Release* **2014**, *183*, 146.
[21] J. Shi, L. Kundrat, N. Pishesha, A. Bilate, C. Theile, T. Maruyama, S. K. Dougan, H. L. Ploegh, H. F. Lodish, *Proc. Natl. Acad. Sci. USA* **2014**, *111*, 10131.
[22] M. Delcea, N. Sternberg, A. M. Yashchenok, R. Georgieva, H. Bäumler, H. Möhwald, A. G. Skirtach, *ACS Nano* **2012**, *6*, 4169.
[23] S. Ahn, S. Y. Jung, E. Seo, S. J. Lee, *Biomaterials* **2011**, *32*, 7191.
[24] N. Huebsch, D. J. Mooney, *Nature* **2009**, *462*, 426.
[25] L. Sun, C.-W. Huang, J. Wu, K.-J. Chen, S.-H. Li, R. D. Weisel, H. Rakowski, H.-W. Sung, R.-K. Li, *Biomaterials* **2013**, *34*, 2107.
[26] G. Yang, H. Gong, X. Qian, P. Tan, Z. Li, T. Liu, J. Liu, Y. Li, Z. Liu, *Nano Res.* **2014**, DOI: 10.1007/s12274-014-0558-0.
[27] X. Yang, X. Liu, Z. Liu, F. Pu, J. Ren, X. Qu, *Adv. Mater.* **2012**, *24*, 2890.
[28] M. P. Melancon, M. Zhou, C. Li, *Acc. Chem. Res.* **2011**, *44*, 947.
[29] Q. Yuan, Y. Wu, J. Wang, D. Lu, Z. Zhao, T. Liu, X. Zhang, W. Tan, *Angew. Chem.* **2013**, *125*, 14215.

[30] K. Yang, L. Feng, X. Shi, Z. Liu, *Chem. Soc. Rev.* **2013**, *42*, 530.
[31] X. Wang, C. Wang, L. Cheng, S. T. Lee, Z. Liu, *J. Am. Chem. Soc.* **2012**, *134*, 7414.
[32] X. Ma, H. Tao, K. Yang, L. Feng, L. Cheng, X. Shi, Y. Li, L. Guo, Z. Liu, *Nano Res.* **2012**, *5*, 199.
[33] Z. Wang, Z. Chen, Z. Liu, P. Shi, K. Dong, E. Ju, J. Ren, X. Qu, *Biomaterials* **2014**, *35*, 9678.
[34] N. Wang, Z. Zhao, Y. Lv, H. Fan, H. Bai, H. Meng, Y. Long, T. Fu, X. Zhang, W. Tan, *Nano Res.* **2014**, *7*, 1291.
[35] C. G. Millan, A. Z. Castaneda, M. L. S. Marinero, J. M. Lanao, *Blood Cells, Mol. Dis.* **2004**, *33*, 132.
[36] B. Bahmani, D. Bacon, B. Anvari, *Sci. Rep.* **2013**, *3*, 2180.
[37] L. Wu, S. Fang, S. Shi, J. Deng, B. Liu, L. Cai, *Biomacromolecules* **2013**, *14*, 3027.
[38] M. Zheng, C. Yue, Y. Ma, P. Gong, P. Zhao, C. Zheng, Z. Sheng, P. Zhang, Z. Wang, L. Cai, *ACS Nano* **2013**, *7*, 2056.
[39] Q. Chen, C. Wang, Z. Zhan, W. He, Z. Cheng, Y. Li, Z. Liu, *Biomaterials* **2014**, *35*, 8206.
[40] E. D. Moody, P. J. Viskari, C. L. Colyer, *J. Chromatogr. B* **1999**, *729*, 55.
[41] A. J. Schroit, J. W. Madsen, Y. Tanaka, *J. Biol. Chem.* **1985**, *260*, 5131.
[42] F. Kuypers, K. De Jong, *Cell. Mol. Biol.* **2004**, *50*, 147.
[43] J.-C. Murciano, S. Medinilla, D. Eslin, E. Atochina, D. B. Cines, V. R. Muzykantov, *Nat. Biotechnol.* **2003**, *21*, 891.
[44] S. Biagiotti, L. Rossi, M. Bianchi, E. Giacomini, F. Pierige, G. Serafini, P. G. Conaldi, M. Magnani, *J. Controlled Release* **2011**, *154*, 306.